

Functionalized surfaces based on polymers and carbon nanotubes for some biomedical and optoelectronic applications

This article has been downloaded from IOPscience. Please scroll down to see the full text article.

2003 Nanotechnology 14 1081

(<http://iopscience.iop.org/0957-4484/14/10/305>)

View [the table of contents for this issue](#), or go to the [journal homepage](#) for more

Download details:

IP Address: 129.22.126.230

The article was downloaded on 02/04/2012 at 23:56

Please note that [terms and conditions apply](#).

Functionalized surfaces based on polymers and carbon nanotubes for some biomedical and optoelectronic applications

Liming Dai¹, Pingang He and Sinan Li

Department of Polymer Engineering, College of Polymer Science and Polymer Engineering,
The University of Akron, 250 S Forge Street, Akron, OH 44304-0301, USA

E-mail: ldai@uakron.edu

Received 1 April 2003, in final form 19 July 2003

Published 27 August 2003

Online at stacks.iop.org/Nano/14/1081

Abstract

It has been long recognized that surface properties are of paramount importance for a broad range of materials and a large variety of devices. The recent development of nanoscience and nanotechnology has opened up novel fundamental and applied frontiers in surface functionalization and characterization. At the nanometre scale, the high surface-to-volume ratio characteristic of most nanomaterials has been demonstrated to have a tremendous influence of many fundamental material properties and device performance. In this paper, we present some of the important issues on the surface functionalization and characterization of polymers and carbon nanotubes for certain biomedical and optoelectronic applications and summarize our recent research activities along this line.

(Some figures in this article are in colour only in the electronic version)

1. Introduction

As is well known, the properties of a broad range of materials and the performance of a large variety of devices depend strongly on their surface characteristics. For instance, it is the surface of a biomaterial/biomedical device that comes into contact with the physiological environment immediately after it is placed in the body or bloodstream and the initial contact regulates its subsequent performance [1]. Likewise, the charge transport process across the interface between a semiconducting polymer film and a metal electrode forms the basis for understanding and improving the performance of many polymeric optoelectronic devices, including thin film transistors [2–4], photovoltaic cells [5] and light-emitting diodes (LEDs) [6]. However, it is very rare that a material with desirable bulk properties also possesses the surface characteristics required for certain specific applications. Therefore, surface modification/functionalization is often

essential in making advanced materials of good bulk and surface properties and devices of desirable features.

With so many advances in both material science and surface analytical techniques within the second half of the last century [7], our understanding of material surfaces has been significantly increased, as with our ability to control and even to tailor the surface characteristics for specific applications. In particular, the turn of this century witnessed the development of a wide range of useful techniques, including photolithography [8], soft-lithography [9], self-assembly [10–12], plasma deposition [13–15] and template syntheses [16, 17] for multidimensional surface microfabrication of various materials. In the meantime, a large number of advanced analytical methods, such as scanned probe imaging [18–20], x-ray photoelectron spectroscopy (XPS) [21], secondary ion mass spectrometry [22] and x-ray/neutron reflectometry [23] have been developed for microanalysis of surface compositions and depth profiles.

The recent development of nanoscience and nanotechnology has opened up novel fundamental and applied

¹ Author to whom any correspondence should be addressed.

frontiers in surface functionalization and characterization. At the nanometre scale, the wave-like properties of electrons inside matter and atomic interactions are influenced by the size of the material [24]. As a consequence, changes in the size-dependent properties (e.g. melting points, magnetic, optic, and electronic properties) may be observed even without any compositional change [24]. Due to the high surface-to-volume ratio associated with nanometre-sized materials, a tremendous improvement in chemical properties is also achievable through a reduction in size [24]. Besides, new phenomena, such as the confinement-induced quantization effect, could also occur when the size of materials becomes comparable to the de Broglie wavelength of charge carriers inside [24]. By creating nanostructures, therefore, it is possible to control the fundamental properties of materials through the surface/size effect. This should, in principle, allow us to develop new materials and advanced devices of desirable properties and functions for numerous applications.

Polymers offer a unique class of materials with the natural length of polymer chains and their morphologies in the bulk, lying precisely at the nanometre length scale [24]. This, together with the large number of possible conformations available to a polymer chain on a surface and/or in the bulk, indicates considerable room for creating polymeric materials of new properties and functions even without any change in their chemical composition. On the other hand, the recent discovery of carbon nanotubes [25] has opened up a new era in material science and nanotechnology. In view of the large number of well-defined carbon-carbon single and double bonds in most carbon nanotubes, carbon nanotube at its very essence is polymeric. Having a conjugated all-carbon structure, carbon nanotubes have indeed been demonstrated to possess some similar optoelectronic characteristics to conjugated polymers. Just as conjugated polymers have widely been regarded as quasi-one-dimensional semiconductors (see for example [26–28]), carbon nanotubes can be considered as quantum wires (for recent reviews, see [29–35]). The interesting electronic and photonic properties, coupled with their unusual molecular symmetries, have made carbon nanotubes very attractive for many potential applications, including as new materials for electron field emitters in panel displays [36], single-molecular transistors [37], scanning probe microscope tips (see for example [38–41]), gas and electrochemical energy storage [42], catalyst and protein/DNA supports [43, 44], molecular-filtration membranes [45] and artificial muscles [46]. For most of the above-mentioned, and many other, applications, it is highly desirable to prepare aligned/micropatterned carbon nanotubes and to modify their surfaces, for example with polymers.

Polymer-nanotube hybrid composites constitute a new class of nanomaterials, which could show properties characteristic of both constituent components with potential synergetic effects. For instance, the use of a carbon nanotube as an electrode in a rectifying heterojunction with a conjugated polymer has been demonstrated to significantly reduce the onset voltage for nonlinear current injection due to an enhancement of the local field at the tip of the nanotubes [47]. Likewise, LEDs based on conjugated polymer/carbon nanotube composites have been shown to exhibit lower current densities and better thermal stabilities

than the corresponding pure polymer devices, as carbon nanotubes enhance the conductivity and act as nanometric heat sinks [48]. Recently, we have prepared large-scale aligned carbon nanotube arrays *perpendicular* to the substrate surface by pyrolysis of iron (II) phthalocyanine (FePc) onto the pristine quartz glass plates [49]. Subsequently, we have also developed microfabrication methods for patterning the aligned carbon nanotubes with a sub-micrometre resolution and for patterned/non-patterned transferral of such nanotube arrays to various other substrates of particular interest (e.g. polymer films for organic optoelectronic devices or metal substrates for electrochemistry) [49–53]. We have also prepared novel aligned conducting polymer-carbon nanotube coaxial nanowires by electrochemically depositing a concentric layer of an appropriate conducting polymer onto the individual aligned carbon nanotubes [54]. Furthermore, the aligned structure allows us to develop a simple, but versatile, approach for chemical modification of carbon nanotubes whilst largely retaining their structural integrity [55]. The resultant carbon nanotubes with a tailor-made surface facilitate the use of carbon nanotubes in various applications, ranging from polymer nanocomposites to biomedical devices [56].

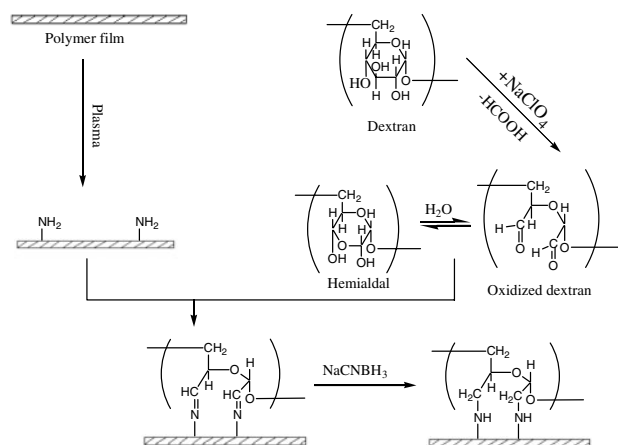
The surface functionalization concerning polymers and carbon nanotubes is a very broad field, which includes material synthesis, structural determination, surface/interface design and modification. In this paper, we present some of the important issues concerning the surface control of polymers and carbon nanotubes for biomedical and optoelectronic applications. Since focus is given to our own work with no intention for a comprehensive literature survey of the subject, there is no doubt that the examples presented in this paper do not exhaust all significant work reported in the literature.

2. Functionalized surfaces with polymer nanofilms

Polymer thin films with their thickness at the nanometre scale (i.e. polymer nanofilms or nanosheets) are an important class of materials from the viewpoints of both the fundamental science and practical applications. For instance, the use of surface-adsorbed polymers is known to be vital for the success of various technological applications and in biological systems, including adhesion, lubrication, steric stabilization of colloidal dispersions and the interaction of cell membranes [57–59]. On the other hand, the use of conjugated polymers in integrated circuits, field-effect transistors, optical memory storage, electroluminescent and electrochromic displays often requires that they be microlithographically patterned on various substrate surfaces [6, 28]. In what follows, we will summarize some of our work on the surface and interface control of polymeric biomaterials and conjugated polymers, though reference is also made to other complementary work as appropriate. Methods for surface micropatterning and region-selective modification will also be discussed.

2.1. Functionalized surfaces with plasma-induced groups and thin films

As is well known, radio-frequency glow-discharge is formed when gaseous monomers are exposed to a radio-frequency electric field at low pressure (<10 Torr) [60, 61]. During



Scheme 1. Periodate oxidation of dextran producing aldehyde groups, followed by covalently grafting the periodate oxidized dextran onto plasma-induced amine surface groups [65].

the glow-discharge process, energy is transferred from the electric field to free electrons, which inelastically collide with molecules leading to generation of more electrons, ions and free radicals in the excited state. These plasma species are very reactive towards surfaces, causing surface modification in the case of plasma treatment and polymer deposition in the case of plasma polymerization. Although the electrons activated for generating charged particles may have a very high electron temperature (e.g. $2\text{ eV} = 23\,200\text{ K}$), they are not at thermodynamic equilibrium with gas molecules in the so-called ‘cold’ plasma process [61]. Therefore, plasma treatment and plasma polymerization can be carried out with the gas molecules being at ambient temperature, and thus without thermal degradation of the sample surface and/or the plasma-polymerized layer. Plasma polymerization has been widely demonstrated to generate thin, cohesive, adhering, pinhole-free polymer thin films, which are often used as protective coatings or adhesion promoting layers and have potential applications in optical waveguides, sensor technology, and electronic/photonics devices [61].

Plasma technique has also played an important role in the surface activation of various materials, ranging from organic polymers to inorganic ceramics and metals [13, 62]. We have developed approaches for the surface modification of biomaterials by plasma techniques. In cases where covalent immobilization of polymer chains is required for chemically inert biomaterials, such as fluorine- and silicon-containing polymers [63], the substrate needs to be pre-activated to introduce suitable reactive surface groups. A popular approach for preparing such activated polymer surfaces is to use the radio-frequency glow-discharge plasma technique for introducing either specific functional surface groups (via plasma treatment) or functional polymer layers (via plasma polymerization) (see for example [60, 61]). Further chemical modification was then achieved by covalently bonding appropriate molecules (e.g. polysaccharides) onto the plasma-activated polymers via various specific reactions between the attaching polymer chains and the plasma-induced surface functional groups. Examples include the attachment of polysaccharides (e.g. dextran, pullulan and blue dextran) onto plasma-induced amine surfaces [63–66]. As can be seen

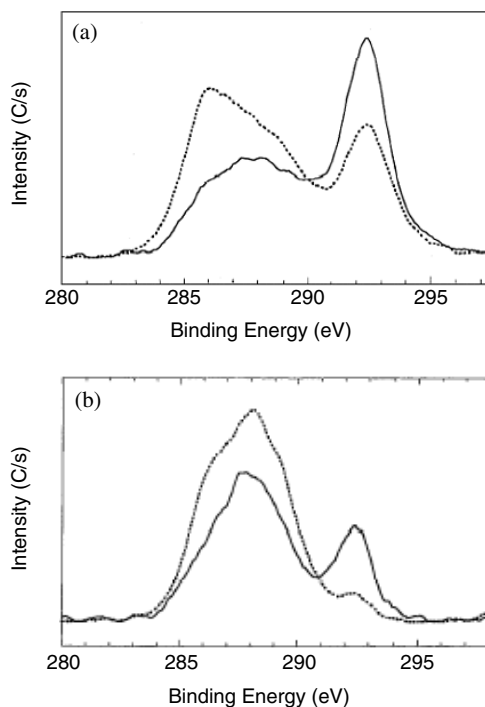


Figure 1. XPS C 1s spectra of (a) NH_3 -plasma-treated FEP recorded at normal emission (0° , solid curve) and glancing emission (75° , dashed curve) and (b) oxidized dextran immobilized onto ammonia-plasma treated FEP, at a photoelectron emission angle of (0° , solid curve) and (75° , dashed curve) [68].

in scheme 1, the immobilization reaction involves oxidation of polysaccharides by sodium metaperiodate, NaIO_4 , to produce aldehyde groups, which were then covalently bound to the plasma-induced surface amine groups to form Schiff bases [65, 66]. After stabilization by NaCNBH_3 , the polymer surface thus modified showed strong, stable hydrophilicity.

The advancing, sessile and receding air/water contact angles (ACA, SCA, RCA) for an untreated perfluorinated ethylene-propylene (FEP) copolymer film are found to decrease from 119° , 107° and 98° to 34° , 25° and 6° , respectively, upon a NH_3 plasma treatment followed by the oxidized dextran attachment. This, together with high water film retention, provides a rapid demonstration of the successful attachment of the hydrophilic polysaccharide coating. While contact angles enable detection of a change in wettability, they do not allow verification that this new surface indeed possesses the composition expected on the basis of the intended reaction. Therefore, XPS analyses were performed [65, 66]. Representative XPS C 1s spectra NH_3 -plasma-treated FEP recorded at normal emission (0°) and glancing emission (75°) are shown in figure 1(a). From comparison with the XPS C 1s spectrum of untreated FEP [67], it becomes clear that the contributions over $284\text{--}289.5\text{ eV}$ are products of the plasma treatment. The outermost surface layer of the FEP had been modified extensively, as attested by the large reduction in the original fluorocarbon signal at 292.5 eV . However, the angle dependence measurements reveals that the plasma layer is thinner than the XPS probe depth (about 10 nm) [68, 69], as the fluorocarbon signal is still observable even at the glancing emission. Figure 1 reproduces XPS C 1s spectra recorded at 0° and 75° emission after the attachment

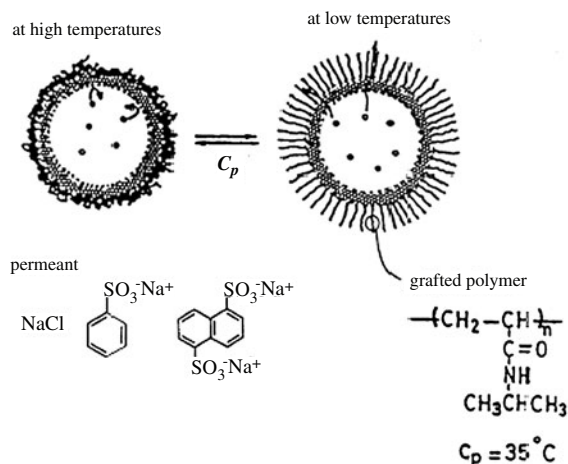


Figure 2. Schematic illustration of the polymer-grafted capsule membrane as a permeation valve [80].

of oxidized dextran onto a FEP/ NH_3 sample. The signals are consistent with expectations based on oxidized dextran superimposed on a FEP/ NH_3 contribution [65–68]. The C 1s signal at glancing emission contains strong C–O and O–C–O components, characteristic of oxidized dextran and a small perfluorocarbon component (at 292.5 eV). The detection of the CF_2 signal from the substrate can occur due to the grafted layer being thinner than the XPS sampling depths.

By end-functionalization of the polysaccharide chains, an end-bound dextran layer has been prepared [70]. In contrast to the side-bound chains, the end-bound polymer brushes could have implications beyond their use as bioinert surfaces because terminally anchored polymer brushes have demonstrated many interesting dynamic and/or kinetic characteristics of importance for the development of new devices (see for example [71–77]). To mention but a few examples: tubular medical devices with their inner surface grafted by certain polymer brushes may act as both sensor and valve for flow control since terminally anchored brush chains can expand in response to a shear flow in a good solvent, leading to a decrease in the cross-sectional area for flow [78, 79]. Alternatively, capsule membranes with end-grafted temperature/pH-responsive polymer chains (e.g. poly(*N*-isopropylacrylamide) or poly(glutamic acid)) may be used as thermoselective drug release devices and/or pH-sensitive gates via a conformational change of the end-grafted polymer brushes (figure 2) [80, 81]. Furthermore, end-adsorbed polymer chains have also been shown to be useful for regulating the frictional forces between solid surfaces, the spreading properties of liquids and the stability of thin films on solid surfaces [82, 83]. In view of the importance of the surface-bound polymer chains to various practical applications, we will elucidate chain conformations and conformational transitions of the surface-bound macromolecules in detail below, using the physically end-adsorbed macromolecules as model systems.

2.2. Functionalized surfaces with end-adsorbed polymer brushes

End-adsorbed polymer brushes have attracted considerable interest in recent years [84–87]. In addition to their potential

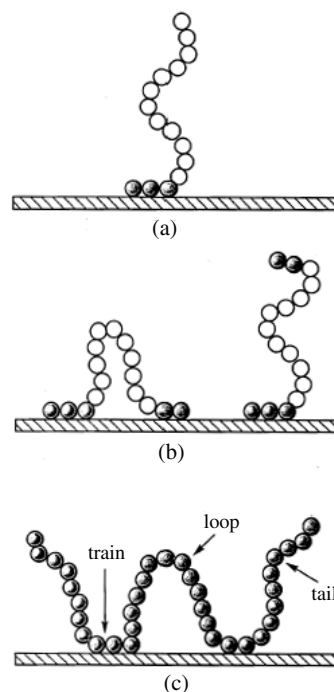


Figure 3. Conformations of adsorbed polymer chains. (a) ‘Tail-like’ conformation of end-adsorbed homopolymer or diblock copolymer. (b) ‘Loop-like’ or ‘tail-like’ conformation of end-adsorbed triblock copolymer. (c) ‘Tail-loop-train’ conformation of adsorbed homopolymer.

use in thermoselective drug release devices and/or pH-sensitive gates [80, 81], the surface-bound polymer brushes have been demonstrated to be of significance for many other technological applications [65, 84–89]. Examples include the use of the end-adsorbed polymer chains for regulating the frictional forces between solid surfaces, the spreading properties of liquids, and the stability of thin films on solid surfaces [82, 83]. Knowledge of macromolecular conformations and conformational transitions of the surface-bound polymer chains is essential for a detailed understanding of their performance at the molecular level. Recent developments, on both experimental and theoretical fronts, in the investigation of adsorbed polymer have brought the goal of structural testing against theories within reach [84–87, 90–93].

Generally speaking, the conformation of polymer chains adsorbed at the liquid/solid interface differs from that in a bulk solution [84–87]. While end-adsorbed homopolymers and diblock copolymers form polymer brushes in which the chains can only exist in a ‘tail’ conformation (figure 3(a)), end-adsorbed triblock copolymers, ABA (the A blocks represent short ‘sticking’ segments, whereas the B block does not adsorb), can form either a ‘loop’ or a ‘tail’ (figure 3(b)) depending on the sticking energy of the A block and the surface coverage at the liquid/solid interface [94]. Adsorbed homopolymer, on the other hand, forms a more complicated conformational structure (figure 3(c)) due to the random adsorption of its constituent monomers onto the surface.

We, along with others, have carried out the structural investigation of adsorbed polymers at the liquid/solid interface using surface force apparatus (SFA) [94–96] and neutron reflectometry (NR) [97–99]. In particular, we have explored

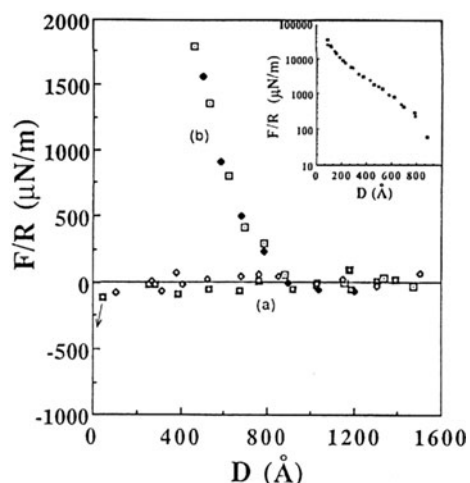


Figure 4. (a) Force–distance profiles between curved mica surfaces in pure toluene for two measurements on two different pairs of mica sheets. (b) Force–distance profiles for an end-adsorbed PS₁₄₂₀–PEO₅₁ diblock copolymer (the subscripts represent weight-averaged degrees of polymerization for polystyrene and poly(ethylene oxide) blocks, respectively) single layer against a *bare* mica surface in toluene. Inset shows the same curve as (b) on a log–linear scale. The solid and open symbols represent compressions and decompressions, respectively [96].

the conformational transitions of the end-adsorbed PS–PEO diblock copolymer chains by directly measuring the interactions of a *single* layer of the end-adsorbed PS–PEO diblock copolymer chains against a *bare* mica surface in pure toluene (good solvent) [94]. The results are given in figure 4, in which no attraction is observed and strong repulsive forces are seen.

Figure 4(a) shows the interaction of two bare mica sheets in toluene. This is always measured before any polymer adsorption is allowed to occur, in order to check that the surfaces are uncontaminated. As expected, figure 4(a) shows little interaction down to a separation, $D \approx 150 \text{ \AA}$, followed by van der Waals like short-range attractions, which eventually cause the mica surfaces to jump into contact. The jump is due to mechanical instability of the leaf spring, which supports the lower mica surface [94]. Figure 4(b) shows the interaction profile of a single adsorbed PS₁₄₂₀–PEO₅₁ diblock layer against a *bare* mica surface in toluene. No attraction is observed at any separation of the surfaces, and strong repulsive forces are seen, commencing at $D \approx 900 \text{ \AA}$. In view of the fact that PEO segments can readily adsorb on the mica surface whereas PS does not adsorb on mica from toluene [94], we conclude that the PS₁₄₂₀–PEO₅₁ chains have been terminally attached to the lower mica surface via the PEO segments, and that the polystyrene chains form a polymer ‘brush’, which shows a repulsive interaction with the upper bare mica surface as it approaches. The force–distance profile given in the inset of figure 4 is the same curve as figure 4(b), but plotted on a log–linear scale over a wide range of separation, which shows clearly about four decades of variation in force. We have also demonstrated that the end-adsorbed PS brush could collapse in the poor solvent (e.g. cyclohexane, $T_\theta = 34 \text{ }^\circ\text{C}$) to form a more compact polymer layer with a thickness of about 200 \AA [94]. The transitions between the polymer ‘brush’ and collapsed layer with changing solvent quality were

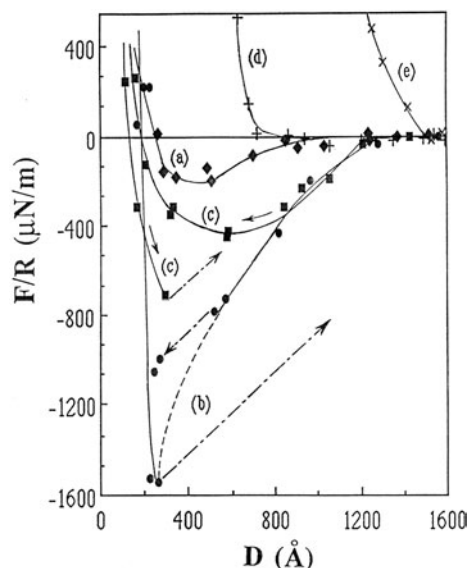


Figure 5. Force–distance profiles between a single PEO–PS–PEO adsorbed layer and a bare mica surface in toluene at different compression–decompression cycles: (a) 6th cycle; (b) 15th cycle; (c) 20th cycle (note the hysteresis between the compression and decompression profiles, indicated by small arrows along each curve); (d) 33rd cycle; (e) 48th cycle. The broken arrows indicate inward and outward jumps due to mechanical instability of the leaf spring supporting the lower mica surface. Approximately 32 h have elapsed between the measurement of the first and last force–distance profiles. Most force profiles corresponding to intermediate numbers of the compression–decompression cycles have been omitted for reasons of clarity [92].

shown to be reversible and characterized by fast dynamics, suggesting potential applications, for example in polymeric valves, sensors and liquid chromatography [100, 101].

The force profiles for a single adsorbed PEO₅–PS₁₂₂₅–PEO₅ triblock copolymer layer against a *bare* mica surface in toluene are shown schematically in figure 5. The clearly detectable attraction forces seen in figures 5(a)–(c) are due to polymer ‘bridges’ formed by the PEO–PS–PEO chains between the mica sheets through simultaneous anchoring of the two PEO end-blocks of a single triblock copolymer chain onto opposing surfaces [102]. Compression–decompression cycles cause evolution of the force profiles from attractive to repulsive, reflecting the conformational rearrangements from a ‘tail’ into a ‘loop’ and the subsequent migration of chains between the mica surfaces (figures 5(d) and (e)). These changes have been confirmed by several recent theoretical calculations [103–109]. These results have potential implications for the use of triblock copolymers either as steric stabilizers (while in a loop conformation) or as flocculants (while in a bridging tail conformation) for dispersed particles.

Although the SFA serves as a good experimental technique for probing conformations and conformational transitions of macromolecular chains within the adsorbed polymer thin film at the liquid/solid interface, the force measurements cannot determine the distribution of segment density normal to the surface. Neutron reflection experiments provide information on the density profile normal to the interface [23, 99]. In

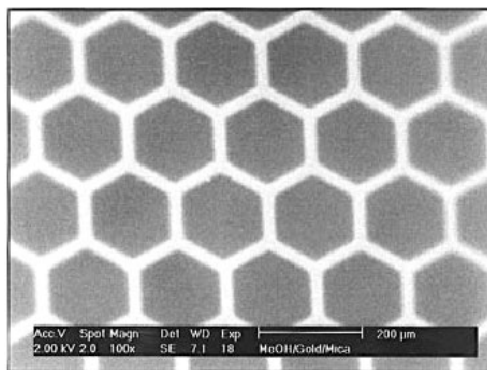


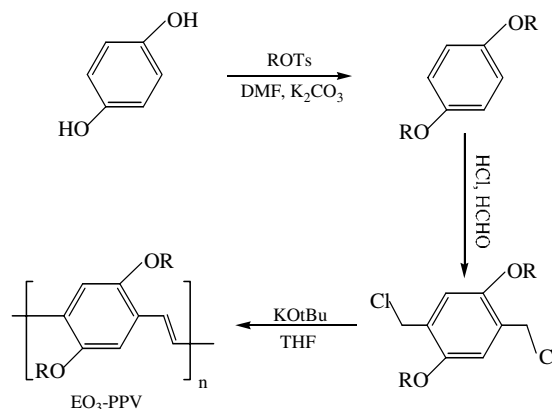
Figure 6. Typical SEM micrograph of the gold-coated mica sheets patterned by the MeOH plasma-polymer with a TEM grid consisting of hexagonal windows as the mask [62].

this regard, we investigated the segment density profiles of the surface-bound polymers normal to the interface by reflectometry, choosing neutrons as the radiation because of important contrast effects, which can operate at the molecular level [99]. For terminally anchored polymer chains in a good solvent, two regimes are anticipated. If the grafting density is low, the tethered chains do not interact with each other and exist as separate ‘mushrooms’. If the grafting density is high, with a distance between anchor points less than the Flory radius of the chains (i.e. $s < R_F$), the polymers take up a more extended configuration to form a semidilute ‘brush’ [97, 98].

In the mushroom regime, each chain may be thought of as occupying roughly a hemisphere, with a radius comparable to the Flory radius for a polymer coil in a good solvent [97, 98]. In the brush regime, however, the segment density profile of an end-adsorbed PS₁₇₀₀–PEO₁₆₇ normal to the interface in a good solvent can be fitted by a parabolic function [103, 104, 110]. More recent NR measurements on telechelic *triblock* copolymer chains by Toprakcioglu and co-workers [111] have demonstrated, to a very good approximation, that ABA-type end-tethered chains behave in a manner equivalent to their AB-type counterparts of half their molecular weight and they adsorb predominantly in a loop conformation for copolymers with sufficiently strong sticking A blocks, consistent with the SFA measurements [94, 102].

2.3. Functionalized surfaces with micropatterned polymer thin films

As can be seen from the foregoing discussion, we have deposited various macromolecular chains with or without biological activity on different surfaces by either covalent immobilization or physical adsorption for specific applications. In all cases, however, these polymer chains are homogeneously immobilized across the substrate surface. Techniques for controlling the architecture of immobilized components on surfaces, including region-specific protein fixation [112–114], should have a wide range of potential applications, for instance in multianalyte biosensors, cell guidance and molecular electronics. As such, pattern formation and recognition by biologically important molecules has recently become a promising new research area. Various techniques have now been developed for region-specific



Scheme 2. Synthesis of EO₃-PPV via a modified Gilch route [R = –(CH₂CH₂O)₃–CH₃] [119].

immobilization of protein(s) onto polymer surfaces with micrometre-order precision [115–117].

2.3.1. Functionalized surfaces with micropatterned polymers by plasma techniques. We have demonstrated that surface patterns of various specific functionalities could be produced by plasma polymerization of appropriate monomers in a patterned fashion [62]. On this basis, we have fabricated micropatterns of hydroxyl groups through plasma polymerization of methanol using a mask (e.g. a TEM grid), as confirmed by both XPS and SEM measurements [62]. Figure 6 shows a typical scanning electron microscopic (SEM) micrograph of the patterns generated on a gold-coated mica surface by the patterned MeOH-plasma polymerization, with the dark areas representing MeOH plasma-polymer and bright regions being the uncovered gold surface [62]. The plasma pattern thus formed is a close replication of the mask (TEM grid) structure with a resolution at the micrometre scale being clearly evident.

With a similar approach, we have also produced a pattern of amine functionalities by plasma polymerization of heptylamine. These patterned functional groups allow one to explore the region-specific immobilization of biologically important macromolecules for many applications, according to various specific grafting reactions characteristic of the plasma-induced functionalities (e.g. scheme 1).

Plasma-patterned surfaces have also been used to directly deposit certain conducting polymers [118]. In particular, we have developed a plasma method for obtaining micropatterns of 2,5-substituted poly(*p*-phenylene vinylene) derivative with methoxy-terminated oligo(ethylene oxide) side chains (i.e. EO₃-PPV, EO₃ = OR = O(CH₂CH₂O)₃CH₃, scheme 2) by first depositing hydrophilic (acetic acid) plasma patterns onto substrates (e.g. FEP copolymer, FEP, films), and then performing selective adsorption from a solution of EO₃-PPV in chloroform [119]. The driving force for the pattern formation in this particular case was attributed to the polar-polar interaction between the oligo(ethylene oxide) side chains of EO₃-PPV and the micropatterned hydrophilic plasma polymer. Under the fluorescence microscope, the EO₃-PPV patterned regions gave fluorescence emissions characteristic of the conjugated structure.

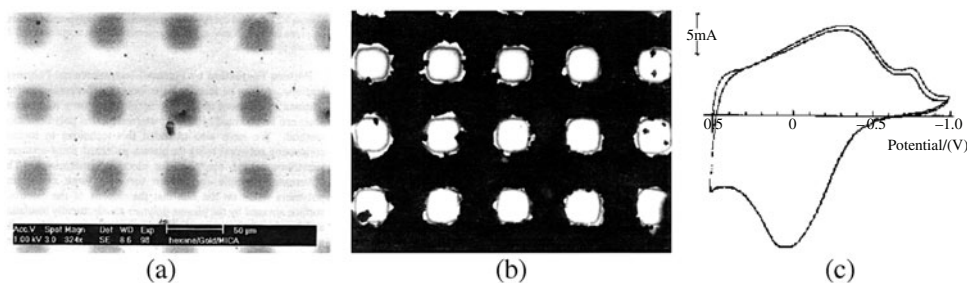
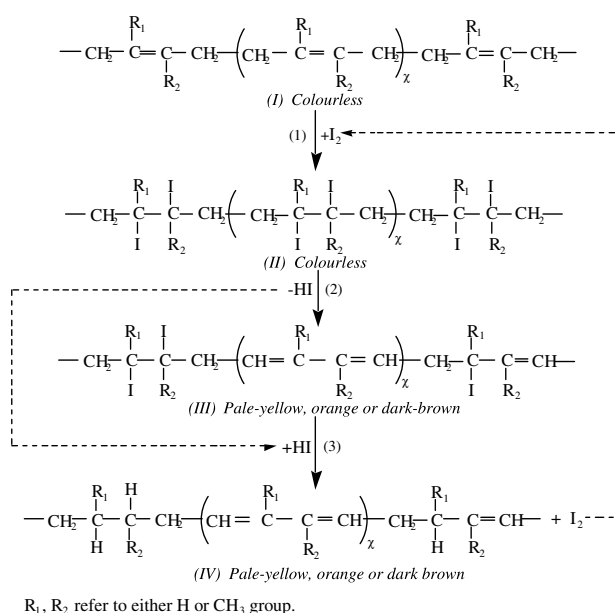


Figure 7. (a) A typical SEM micrograph of gold-coated mica sheets patterned by the *n*-hexane plasma-polymer using a TEM grid as the mask. (b) Optical microscopy image of a polypyrrole pattern electrochemically polymerized onto a platinum-coated mica surface pre-patterned by the *n*-hexane plasma-polymer. (c) A typical cyclic voltammogram of the polypyrrole patterns on platinum at 100 mV s⁻¹ in sodium perchlorate (0.1 M)/H₂O [62].

We have also developed a versatile method for preparing patterned conducting polymers. In so doing, we firstly deposited a thin patterned nonconducting plasma polymer layer (e.g. *n*-hexane plasma film) onto a metal-sputtered electrode, and then performed electropolymerization of monomers (e.g. pyrrole and aniline) within the regions not covered by the patterned plasma-polymer layer [62].

Figure 7(a) shows the surface pattern generated by the patterned plasma polymerization of *n*-hexane on a gold-coated mica surface. A typical reflection light microscopic image of a polypyrrole pattern electrochemically polymerized onto platinum-coated mica sheets pre-patterned with the *n*-hexane plasma-polymer is given in figure 7(b). Comparison with figures 7(a) and (b) shows the same features as the plasma pattern, but with an inverse image contrast. The bright regions characteristic of the uncovered metal surface in figure 7(a) become dark in figure 7(b) due to the presence of a dark layer of the newly polymerized polypyrrole film. The cyclic voltammetric response of the polypyrrole pattern shown in figure 7(b) is given in figure 7(c), which shows a quasi-reversible redox process with two reduction peaks in an aqueous solution of sodium perchlorate. The first reduction peak of figure 7(c) is attributable to the polarons in the electrochemically doped polypyrrole film. On the other hand, the second reduction peak has been known to be associated with the coexistence of a dicationic species (i.e. bipolarons) [62]. Therefore, the cyclic voltammogram measurements indicate that the polypyrrole patterns thus produced are electrochemically active.

Although the advantages of the plasma patterning of semiconducting polymer thin films for electronic applications remains to be demonstrated, an oxygen or nitrogen plasma treatment of a PPV layer at the PPV/Al interface in a LED device with the Cr/PPV/Al structure has been demonstrated to cause the disappearance of the rectifying behaviour and an increase in the current by many orders of magnitude [120]. Similarly, the efficiency, brightness, and lifetime of LEDs were shown to be significantly improved by an air or argon plasma treatment on the ITO surface, presumably due to the removal of organic residue coupled with an increase in the work function of ITO [121, 122]. Hydrogen plasma, on the other hand, was found to increase the turn-on voltage and reduce the efficiency largely due to a decrease in the work function of ITO [121–124]. Thus, the plasma technique shows much promise for interfacial engineering in LEDs [123, 124].



Scheme 3. Reactions of polydiene with iodine, leading to the formation of conjugated sequences [129]. Reaction (3) most likely proceeds by the free radical mechanism (see: [126]): I₂ ⇌ 2I; I + RI ⇌ R + I₂; R + HI ⇌ RH + I; where RI and RH represent polymer (III) and polymer (IV), respectively.

Furthermore, some studies have reported the use of plasma polymers as emitting layers in LED devices [125]. There is no doubt that the plasma surface modification and patterning demonstrated above will have potential implications for making novel electronic and photonic devices. The ease with which multilayered polymer nanofilms of organic materials can be made by the plasma technique could provide additional benefits to this approach [118].

2.3.2. Functionalized surfaces with micropatterned polymers by photolithography. As is well known, photolithographic processing has been widely used for micropattern formation in the semiconductor industries (e.g. for delineating the circuit elements in today's large-scale integrated devices) for many years [127]. Photolithographic patterning of conducting polymers, however, is a recent development [128].

In our further investigation of conducting polydienes [129], we have found that *cis*- and *trans*-1,4-polybutadiene exhibit different behaviour towards the reactions of scheme 3.

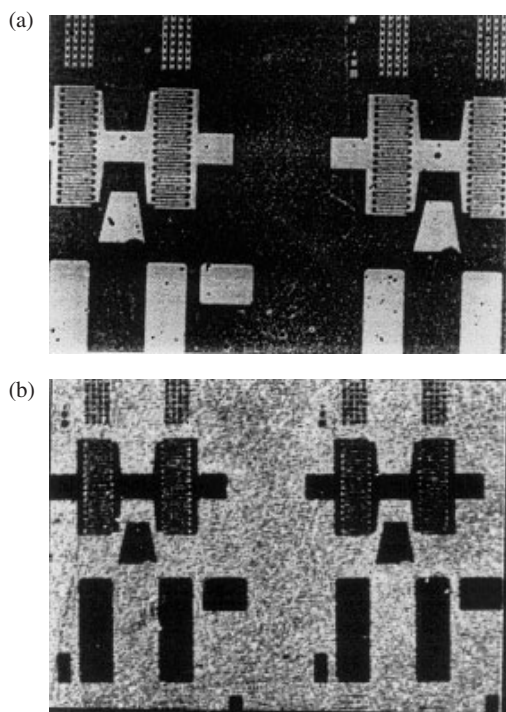


Figure 8. (a) Optical microscopy image of a pattern obtained by 'I₂-doping' of the photoisomerized *trans*-1,4-polybutadiene regions in the iodinated *cis*-1,4-polybutadiene matrix. The dark areas are regions of 'I₂-doped' polybutadiene, and the width of the white rectangles at the bottom part of the picture is 18 μm. (b) Fluorescence micrograph of the conducting pattern [129].

For *cis*-1,4-polybutadiene the reaction sequence given in scheme 3 terminated, at room temperature, at product (II), whereas for the *trans*-isomer the reaction sequence proceeded towards product (III) and/or (IV) thus leading to the formation of conjugated sequences which confer electrical conductivity. Spectroscopic measurements and molecular orbital calculations demonstrated that it was an unfavourable combination of electronic and steric interactions within the iodinated *cis*-1,4-polybutadiene backbone (product II) that inhibited the elimination of hydrogen iodide through the E-2 elimination mechanism (reaction (2) of scheme 3) at room temperature, and hence halted the formation of conjugated sequences in the case of *cis*-1,4-polybutadiene [129–132].

However, *cis*-1,4-polybutadiene can be photoisomerized into the *trans*-isomer [133], and the isomerized material is then amenable to 'I₂-doping'. This discovery provides means for photolithographic generation of conducting patterns from *cis*-1,4-polybutadiene films through region-specific photoisomerization of the *cis*-isomer into its *trans*-counterpart and subsequent I₂-induced conjugation of the photoisomerized *trans*-1,4-polybutadiene chains [129]. The conducting patterns thus formed are coloured and show strong fluorescence emission, which enables visualization of the conducting polymer regions. An example of the conducting patterns thus generated is shown in figure 8(a). It is a close replication of the photomask structure, and conducting wires on a micrometre scale are clearly evident. A corresponding fluorescence microscopic image of the conducting pattern is given in figure 8(b). It shows the same features as the optical micrograph (figure 8(a)), but with

inverse intensities in the image. The dark regions characteristic of the 'I₂-doped' *trans*-1,4-polybutadiene in figure 8(a) gave rise to bright fluorescence emission in figure 8(b), consistent with the fluorescence emission originating from the conjugated structures [134, 135]. The dark regions in figure 8(b) represent non-fluorescent components associated with the *cis*-isomer. The ease with which the conducting micropatterns can be generated and the fact that *cis*-1,4-polybutadiene can easily be spin coated, solvent cast onto various substrates, or even melt extruded into thin free-standing films offer possibilities for novel applications of polybutadiene rubber in, for example, micro-/nano-electronic devices.

3. Functionalized surfaces with carbon nanotubes and their polymeric derivatives

Carbon nanotubes can be viewed as a graphite sheet rolled up into a nanoscale tube form (single-wall carbon nanotubes, SWNTs) [136, 137] or with additional graphene tubes around the core of a SWNT (multi-wall carbon nanotubes, MWNTs) [138]. These elongated nanotubes usually have a diameter in the range of between a few ångströms and tens of nanometres and a length of up to several centimetres with both ends of the tubes normally capped by fullerene-like structures containing pentagons. They can exhibit semiconducting or metallic behaviour depending on their diameter and helicity of the arrangement of graphitic rings in the walls [139–142]. Dissimilar carbon nanotubes may be joined together, allowing the formation of molecular wires with interesting electrical, magnetic, nonlinear optical, and mechanical properties attractive for a variety of potential applications [29, 143].

As mentioned earlier, it is highly desirable to prepare ordered/micropatterned carbon nanotubes so that the properties of individual nanotubes can be probed and they can be effectively incorporated into devices. Below, we will summarize some of our recent work on micropatterning and surface modification of carbon nanotubes.

3.1. Functionalized surfaces with aligned carbon nanotubes

Although carbon nanotubes synthesized by most of the common techniques, such as arc discharge and catalytic pyrolysis (for recent reviews, see [29–35]), often exist in a randomly entangled state (figure 9(a)) [48, 144], aligned carbon nanotubes have been prepared either by post-synthesis fabrication (see for example [145, 146]) or by synthesis-induced alignment [56]. In this regard, we have prepared aligned carbon nanotubes by pyrolyzing FePc and the detailed procedures for the aligned nanotube growth have been reported previously (see for example [49, 147]). Without repetition of the detailed discussions on the synthesis and structural characterization, a typical SEM image of the FePc-generated aligned carbon nanotube array after having been transferred onto a gold foil is shown in figure 9(b). As can be seen, the constituent nanotubes in the perpendicularly aligned carbon nanotube array have a fairly uniform length. Elsewhere, we have also demonstrated that these aligned carbon nanotubes possess a well-graphitized structure with about 50 concentric carbon shells and an outer diameter of about 40 nm [148].

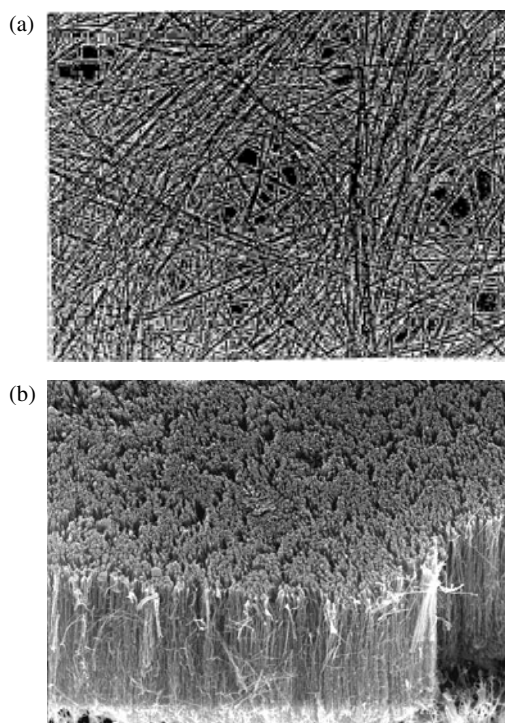


Figure 9. (a) A typical TEM image of an oxidation-purified carbon nanotube sample generated by the arc discharge method. (b) A typical SEM image of the aligned carbon nanotube arrays of about 20 μm long prepared by the pyrolysis of FePc.

3.2. Functionalized surfaces with micropatterned carbon nanotubes

Apart from the aligned carbon nanotubes described above, certain applications (e.g. electron emitters for panel display, sensor arrays) may require the carbon nanotubes to be patterned onto various substrates, in a similar fashion as silicon or metals in semiconducting devices. In what follows, we will present an overview of our recent work on the patterning and surface modification of carbon nanotubes.

3.2.1. Functionalized surfaces with plasma-pattered non-aligned carbon nanotubes. We have developed a versatile method for making patterns of non-aligned carbon nanotubes [52]. In so doing, we first generated plasma-induced (either by non-depositing plasma treatment or by plasma polymerization) surface patterns of $-\text{NH}_2$ groups onto a substrate (e.g. quartz glass plate, mica sheet, polymer film), and then performed region-specific adsorption of the COOH-containing carbon nanotubes from an aqueous medium through the polar-polar interaction between the COOH groups and the plasma-patterned $-\text{NH}_2$ groups. The COOH-containing carbon nanotubes were prepared by acid treatment (HNO_3) of the FePc-generated nanotubes [149].

Figure 10 reproduces a SEM image of the COOH-containing carbon nanotubes region-specifically adsorbed (about 2.5 mg/10 ml H_2O) onto a mica sheet pre-patterned with the heptylamine plasma polymer (200 kHz, 10 W, and a monomer pressure of 0.13 Torr for 30 s). The adsorbed carbon nanotubes are clearly evident by inspection of the plasma-patterned areas of figure 10 under a higher magnification

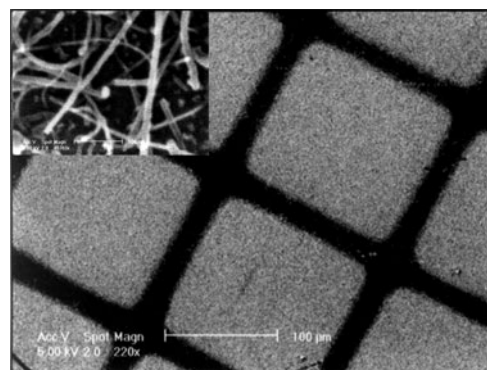


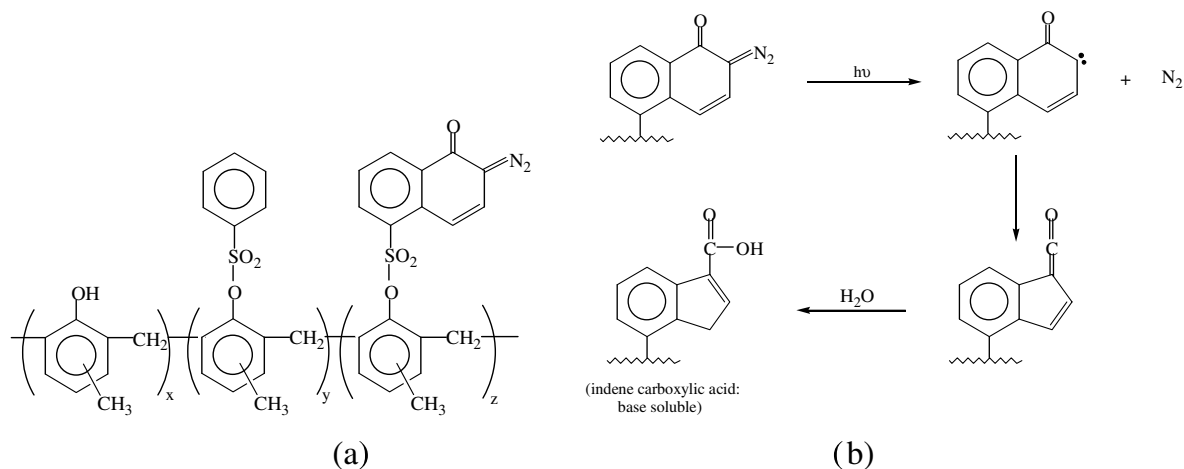
Figure 10. SEM images of adsorbed COOH-containing carbon nanotubes (within the squared areas) on a heptylamine plasma patterned mica sheet. Inset: a higher-magnification image of the plasma-covered areas, showing the individual adsorbed carbon nanotubes [52].

(inset of figure 10). The corresponding high-magnification SEM image for the plasma-polymer-free areas reveals an almost featureless smooth surface characteristic of mica sheet. No adsorption of the carbon nanotubes was observed in a control experiment when a pure mica sheet was used as the substrate.

3.2.2. Functionalized surfaces with aligned carbon nanotube patterns by lithography.

On our further investigation of the aligned carbon nanotubes produced by the pyrolysis of FePc, we, among others [150–153], have recently developed a novel method for photolithographic generation of the perpendicularly aligned carbon nanotube arrays with resolutions down to a micrometre scale [50]. Our method allows not only the preparation of micropatterns and substrate-free films of the perpendicularly aligned nanotubes but also their transfer onto various substrates, including those which would otherwise not be suitable for nanotube growth at high temperatures (e.g. polymer films) [49]. Figure 11(a) shows the steps of the photolithographic process. In practice, we first photolithographically patterned a positive photoresist film of diazonaphthoquinone (DNQ)-modified cresol novolak (scheme 4(a)) onto a quartz substrate. Upon UV irradiation through a photomask, the DNQ-novolak photoresist film in the exposed regions was rendered soluble in an aqueous solution of sodium hydroxide due to photogeneration of the hydrophilic indenecarboxylic acid groups from the hydrophobic DNQ via a photochemical Wolff rearrangement [154] (scheme 4(b)). We then carried out the pyrolysis of FePc, leading to region-specific growth of the aligned carbon nanotubes in the UV exposed regions (figure 11(b)). In this case, the photolithographically patterned photoresist film, after an appropriate carbonization process, acts as a shadow mask for the patterned growth of the aligned nanotubes, most probably because surface properties of the carbonized polymer layer became unsuitable for the segregation of Fe nanoparticles required for the nanotube growth [148]. This method is fully compatible with existing photolithographic processes [8, 155].

Subsequently, we found that 3D micropatterns of well-aligned carbon nanotubes can also be prepared by pyrolysis of FePc onto appropriate photo-patterned substrates [53]. In this particular case, the photopatterning was achieved by photolithographic crosslinking of a chemically amplified



Scheme 4. (a) Molecular structure of the DNQ-novolak photoresist and (b) photochemical reactions of the DNQ-novolak photoresist [50].

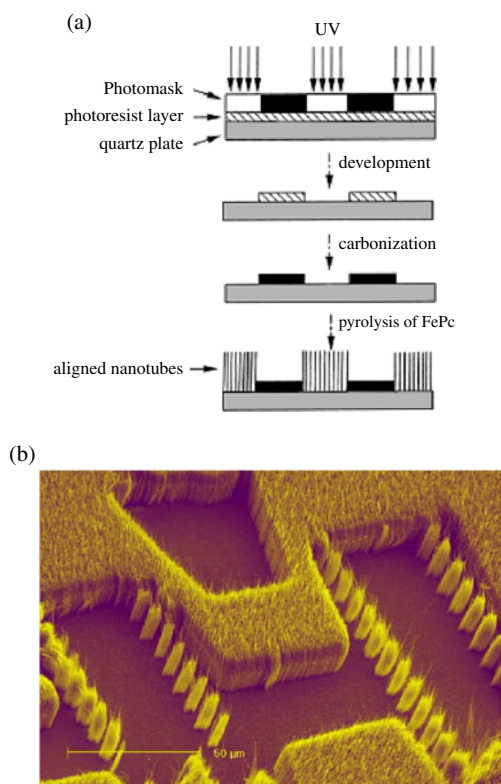


Figure 11. (a) Schematic representation of the micropattern formation of aligned carbon nanotubes by the photolithographic process. (b) Typical SEM micrographs of patterned films of aligned nanotubes prepared by the pyrolysis of FePc onto a photolithographically pre-patterned quartz substrate [50].

photoresist layer spin-cast on a quartz plate or a Si wafer, coupled with a solution development to generate a negative photoresist pattern. Owing to an appropriate surface characteristic, the patterned photoresist layer was found in this case to support the aligned carbon nanotube growth by pyrolysis of FePc, as were the photoresist-free substrate surfaces. The difference in chemical nature between the surface areas covered and uncovered by the photoresist film, however, caused a region-specific growth of the nanotubes with different tubular lengths and packing densities (figure 12).

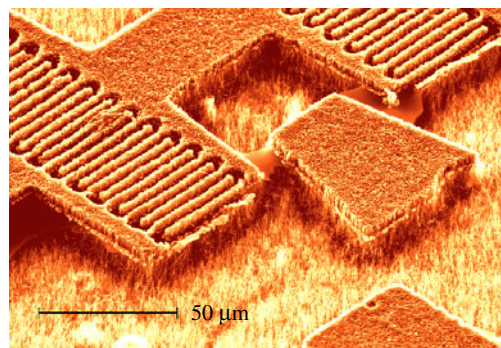


Figure 12. Typical SEM micrographs of the 3D aligned carbon nanotube micropattern [53].

More recently, we have also used the micro-contact printing (μ CP) and micro-moulding techniques to prepare micropatterns of carbon nanotubes aligned in a direction normal to the substrate surface [51]. While the μ CP process involves the region-specific transfer of self-assembling monolayers (SAMs) of alkylsiloxane onto a quartz substrate and subsequent adsorption of polymer chains in the SAM-free regions (figure 13(a)), the micro-moulding method allows the formation of polymer patterns through solvent evaporation from a precoated thin layer of polymer solution confined between a quartz plate and a polydimethylsiloxane (PDMS) elastomer mould (figure 13(b)). The DNQ-novolak photoresist patterns formed in both cases were then carbonized into carbon black for region-specific growth of the aligned nanotubes in the polymer-free regions by pyrolysis of FePc under Ar/H₂ atmosphere at 800–1100 °C, as is the case for the above-mentioned photolithographic patterning. The spatial resolution is limited by the resolution of the mask used. Micropatterns of aligned nanotubes thus prepared have resolutions down to 0.8 μ m (figure 13(c)), suitable for fabrication of various electronic and photonic devices. The ease with which micro-/nano-patterns of organic materials can be made on curved surfaces by the soft lithographic techniques [9, 156] should provide additional benefits to this approach with respect to the photolithographic method, especially for the construction of flexible devices.

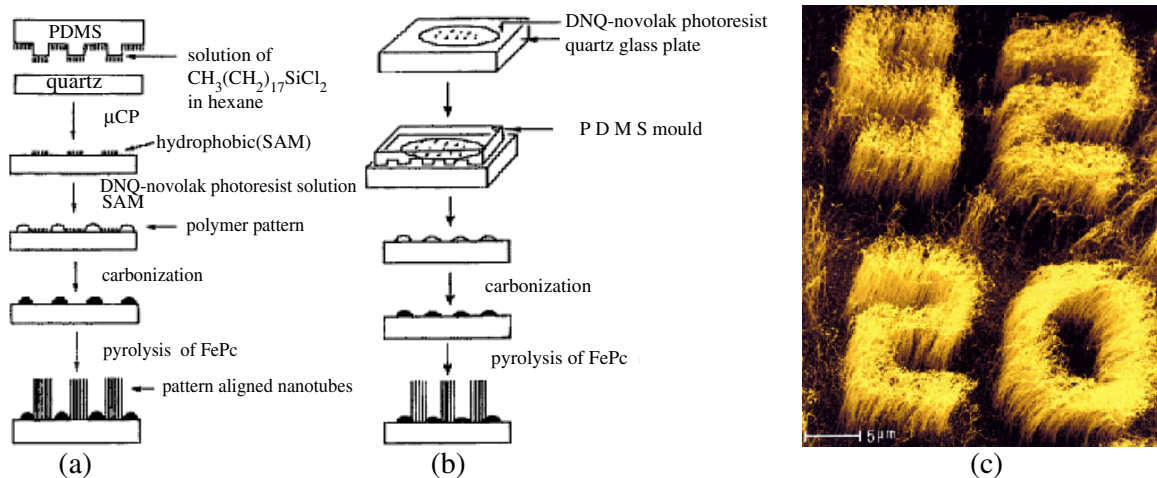


Figure 13. Schematic illustration of the procedure for fabricating patterns of aligned carbon nanotubes by (a) microcontact printing; (b) solvent-assisted micromoulding; (c) a typical SEM image of aligned nanotube pattern prepared by the pyrolysis of FePc onto the photoresist pre-patterned quartz via the micromoulding technique [51].

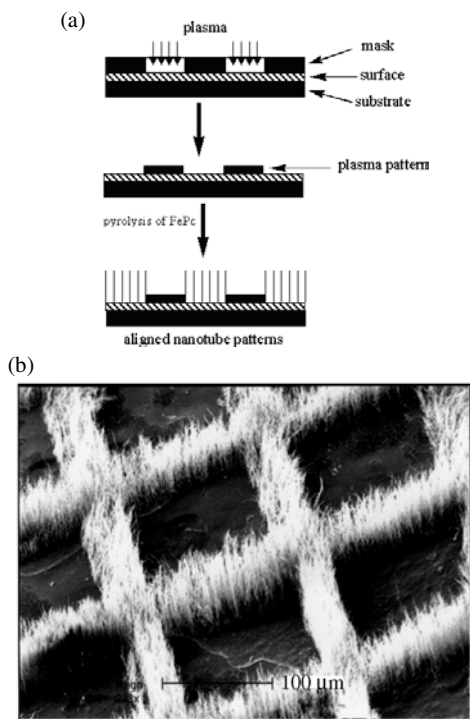


Figure 14. (a) Schematic illustration of the procedure for fabricating patterns of carbon nanotubes by plasma polymerization followed by nanotube growth; (b) a typical SEM image of aligned nanotube arrays growing out from the plasma-polymer-free regions on an *n*-hexane-plasma-polymer-patterned quartz plate [52].

3.2.3. Functionalized surfaces with plasma-patterned aligned carbon nanotubes. As can be seen from the above discussion, both the photolithographic and soft-lithographic patterning methods involve a tedious carbonization process prior to the aligned nanotube growth. In order to eliminate the carbonization step, we have also developed a versatile plasma method for making patterns of aligned carbon nanotubes [52]. In this case, we first polymerized certain plasma polymers in a

region-specific fashion using a TEM grid as the physical mask (figure 14(a)). The highly crosslinked structure of plasma-polymer films [13, 62] could ensure the integrity of the plasma polymer layer to be maintained, even without carbonization, at high temperatures necessary for the nanotube growth from FePc [52]. Therefore, the carbonization process involved in our previous work on photolithographic [50] and soft-lithographic [51] patterning of the aligned carbon nanotubes can be completely eliminated in the plasma patterning process. Owing to the generic nature characteristic of the plasma polymerization, many other organic vapours could also be used equally well to generate plasma polymer patterns for the patterned growth of the aligned carbon nanotubes. Figure 14(b) shows a SEM image of the aligned nanotube micropatterns prepared on an *n*-hexane-plasma-polymer pre-patterned quartz plate.

As can be seen from above discussion, micropatterns of aligned nanotubes with resolutions down to the sub-micron scale, suitable for fabrication of various electronic and photonic devices, have been prepared by lithographic and/or plasma techniques. These lithographic/plasma patterning methods, coupled with the ease with which polymer chains can be chemically and/or electrochemically attached onto the carbon nanotube wall, should allow the formation of the nanostructured polymer–nanotube coaxial nanowires in a patterned fashion, attractive for constructing various on-tube optoelectronic devices and sensor arrays, as we shall see later.

3.3. Functionalized surfaces with polymer-coated aligned carbon nanotubes

3.3.1. Functionalized surfaces with plasma-polymer-coated aligned carbon nanotubes. The aforementioned aligned and micropatterned carbon nanotubes are ideal for use as electron field emitters in panel displays. We have recently carried out an investigation of the influence of the plasma polymerization on the electron emission from the aligned carbon nanotubes. Some of the results are presented here.

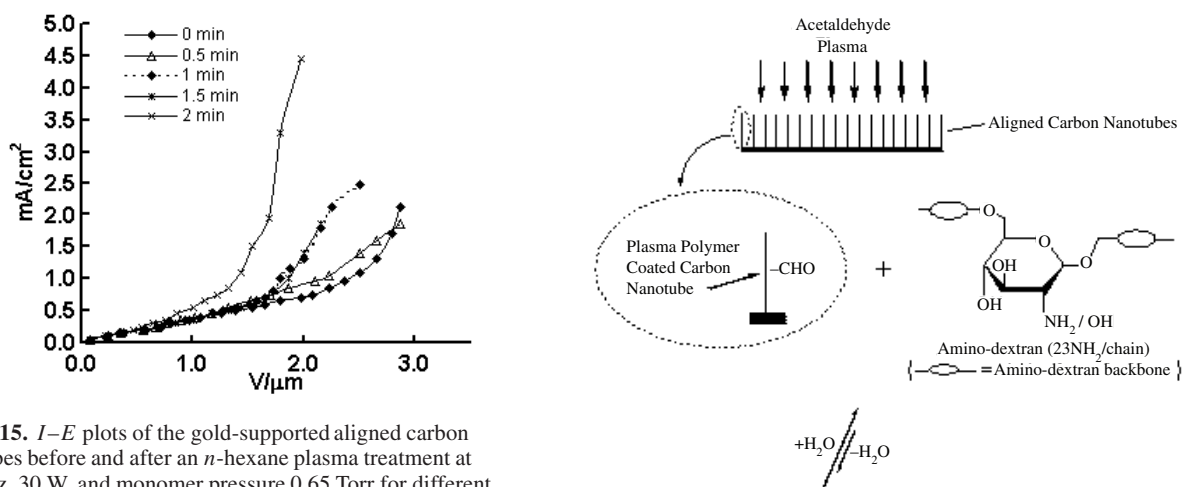


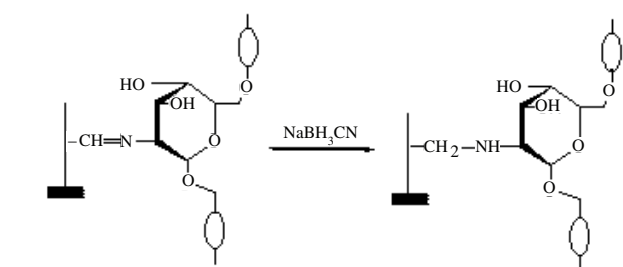
Figure 15. I - E plots of the gold-supported aligned carbon nanotubes before and after an n -hexane plasma treatment at 250 kHz, 30 W, and monomer pressure 0.65 Torr for different periods of time [159].

The carbon nanotube electron emitters work on a similar principle to a conventional cathode ray tube, but their small size could lead to a thinner, more flexible and energy efficient display screen with a higher resolution. The field emission study on SWNTs carried out by de Heer *et al* [157] showed some promising results with the turn-on field E_{10} (defined as the electric field required to emit a current $I = 10 \mu\text{A cm}^{-2}$) in the range of 1.5 – $4.5 \text{ V } \mu\text{m}^{-1}$. These values, like those for most MWNTs, are far lower than corresponding values for other film emitters.

To construct aligned carbon nanotube arrays on conducting electrodes for electron emission and electrochemical polymerization (see below), a thin layer of gold was sputter-coated onto the amorphous carbon layer covering an *as-synthesized* aligned nanotube film. We have previously observed that films of the aligned carbon nanotubes produced from FePc were sometimes covered by a thin layer of amorphous carbon film [158]. The gold-covered carbon nanotube film was then separated from the quartz glass plate used for the nanotube growth with an aqueous solution of 30% HF [49]. The transferred nanotubes were still aligned perpendicularly, allowing plasma treatment of individual nanotubes with minimized inter-tube interference [55].

Figure 15 shows changes in the I - E curves for the gold-supported aligned carbon nanotubes upon hexane plasma treatment. As can be seen, hexane-plasma coating reduces the turn-on electric field E_{10} , coupled with a concomitant increase in the emission current at a constant V . Notably, the turn-on electric field decreased from $E_{10} = 2.5 \text{ V } \mu\text{m}^{-1}$, characteristic of the pristine aligned carbon nanotubes, to $E_{10} = 1.5 \text{ V } \mu\text{m}^{-1}$, with a significant increase in the emission current at a constant V after being treated with the n -hexane plasma for 2 min [159]. We believe that the enhanced field emission by the hexane-plasma treatment is originated from the electrical insulating of the nanotubes along their length, leading to an enhanced field focusing at the nanotube tips.

3.3.2. Functionalized surfaces with polysaccharide-grafted aligned carbon nanotubes. As seen above, certain applications may inevitably require the surface modification of carbon nanotubes. Therefore, a large number of



Scheme 5. Grafting polysaccharide chains onto plasma-activated aligned carbon nanotubes through Schiff-base formation, followed by reductive stabilization of the Schiff-base linkage with sodium cyanoborohydride [55].

solution methods have been reported to modify nanotube tips and sidewalls through either covalent or non-covalent chemistries [35]. A simple application of the solution chemistry to the aligned carbon nanotubes, however, could cause a detrimental damage to their alignment structure. The plasma method offers a particularly attractive option for chemical modification of carbon nanotubes whilst largely retaining their structural integrity. In this regard, we have developed approaches for chemical modification of aligned carbon nanotubes by carrying out radio-frequency glow-discharge plasma treatment, and subsequent reactions characteristic of the plasma-induced surface groups [55]. For instance, we have successfully immobilized NH₂-containing polysaccharide chains onto acetaldehyde plasma-activated carbon nanotubes through the Schiff-base formation, followed by reductive stabilization of the Schiff-base linkage with sodium cyanoborohydride (scheme 5).

The resulting amino-dextran grafted nanotube film showed zero air/water contact angles. The (acetaldehyde) plasma-treated carbon nanotube film gave relatively low advancing (90°), sessile (78°), and receding (45°) air/water contact angles comparing to the advancing (155°), sessile (146°), and receding (122°) angles for an untreated sheet of aligned carbon nanotubes. The glucose units within the surface-grafted amino-dextran chains (scheme 5) can be further converted into dialdehyde moieties by periodate oxidation [68], thereby, providing considerable room for further chemical modification.

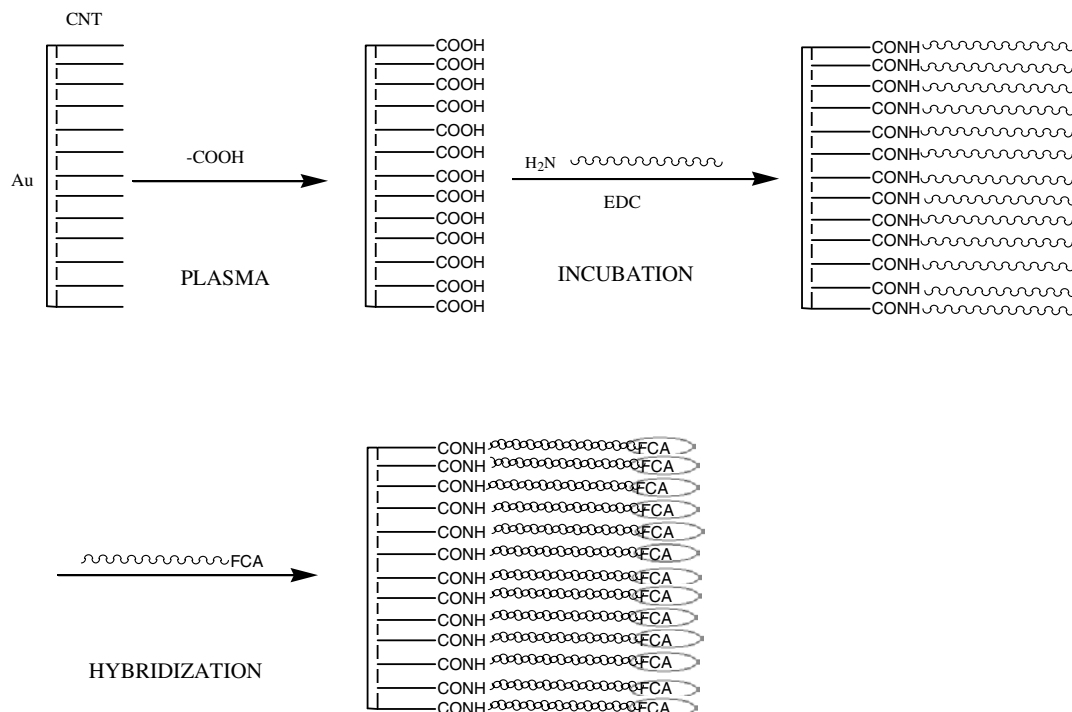


Figure 16. Schematic illustration of fabricating an aligned CNT electrochemical DNA sensor. For reasons of clarity, only the carboxyl groups at nanotube tips are shown.

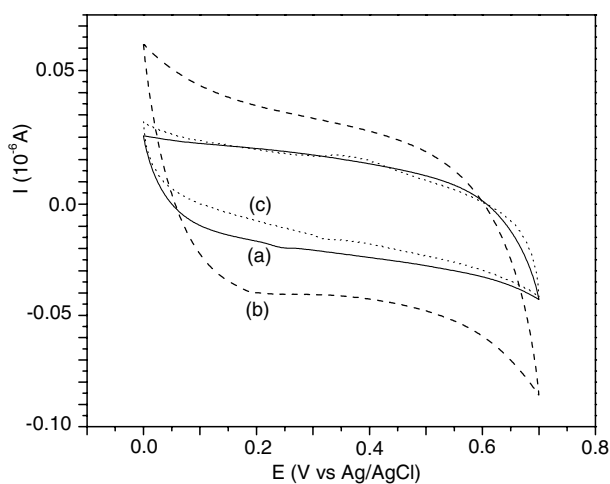


Figure 17. Cyclic voltammograms of (a) the pristine aligned carbon nanotube electrode, (b) the nanotube electrode after the acetic acid plasma treatment at 200 kHz, 20 W, and monomer pressure 0.1 Torr for 5 min and (c) the plasma-treated nanotube electrode after the immobilization of ssDNA. All the cyclic voltammograms were recorded in 0.1 M H_2SO_4 blank solution. Scan rate: 0.1 V s^{-1} , potential window: 0.0–0.8 V (versus Ag/AgCl).

3.3.3. Functionalized surfaces with DNA-grafted aligned carbon nanotubes. The above demonstration of the surface-grafting of amino-dextran chains on the plasma-activated aligned carbon nanotubes prompted us to use the aligned carbon nanotube arrays as a nanoscale platform to build high performance sensors/sensor arrays by surface templating various biomacromolecules and/or conducting polymers onto the nanotube structure. The large surface area, coupled with the good charge transport property, makes the aligned carbon

nanotubes ideal electrodes for constructing electrochemical DNA sensors. DNA hybridization biosensor technologies are currently under intense investigation owing to their high sensitivity, low cost and good compatibility with micro-fabrication technology. Consequently, DNA electrochemical biosensors have been reported by many investigators [160–164]. It was found that the sensitivity of DNA biosensors depends strongly on how intimate is the connection between the nucleic acid chains and electronic transducer.

In view of the covalent-bonding nature characteristic of the plasma activation approach, we developed a novel approach for chemical grafting single-strand DNA (ssDNA) with an amino group at the 5'-phosphate end (i.e. $[\text{AmC6}]\text{TTGACACCAGACCAACTGGT-3'}$) onto the aligned carbon nanotubes treated with acetic acid plasma through the amide formation in the presence of EDC coupling reagent [165]. A complementary DNA (cDNA) chain pre-labelled with ferrocenecarboxaldehyde, FCA, (designated as $[\text{FCA-C6}]\text{ACCAGTTGGTCTGGTGTCAA-3'}$) was then used to hybridize with the surface-immobilized oligonucleotides to form a double strand DNA (dsDNA) on the surface of the aligned carbon nanotubes (figure 16).

Owing to its good electrochemical redox properties, ferrocene has been widely used as an electrochemical mark for DNA biosensors [166, 167]. The FCA labelling allows the hybridization reaction to be followed simply by measuring the redox responses characteristic of the FCA moieties through the nanotube electrode. Figure 17 shows the electrochemical characteristics for the pristine aligned carbon nanotubes before (curve (a)) and after (curve (b)) the acetic-acid-plasma treatment as well as the ssDNA-immobilized nanotubes (curve (c)) in 0.1 M electrolyte H_2SO_4 solution. As can be seen from curve (a) of figure 17, only capacitive current

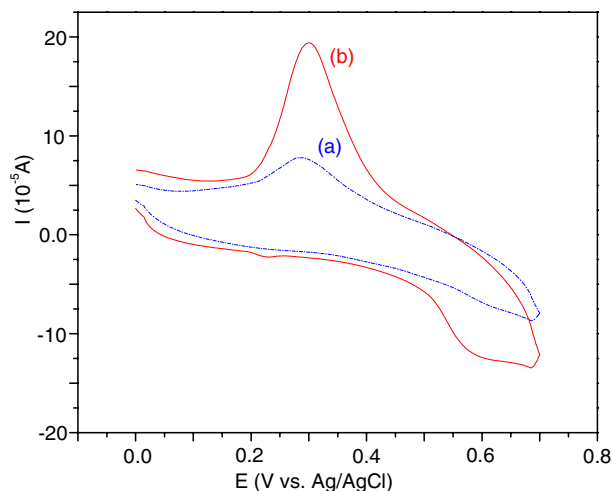


Figure 18. Cyclic voltammograms of the acetic-acid-plasma-treated aligned carbon nanotube electrodes after the immobilization of the ssDNA chains and the subsequent hybridization of the FCA-labelled cDNA chains. (a) Plasma treatment for 1 min, (b) plasma treatment for 5 min. The measurements were carried out in 0.1 M H₂SO₄ blank solution with 0.05 $\mu\text{g ml}^{-1}$ of the FCA labelled cDNA probe. Scan rate: 0.1 V s⁻¹, potential window: 0.0–0.8 V (versus Ag/AgCl).

was observed for the pristine aligned carbon nanotubes. The capacitive current increased after treating the nanotube electrode with the acetic acid plasma (curve (b) of figure 17), most probably because the plasma-induced carboxyl groups facilitated the charge transfer from H₂SO₄ electrolyte to the nanotube electrode through the enhanced hydrophilic–hydrophilic interaction since the pristine nanotube surface, in contrast to the plasma surface, is very hydrophobic [55]. Upon grafting the ssDNA chains onto the plasma-induced surface carboxyl groups, a significant decrease in the capacitive current was observed (curve (c) in figure 17), indicating the replacement of the surface carboxyl groups by a thin layer of the covalently grafted DNA chains.

The presence of the surface-bound ssDNA chains on the plasma-treated nanotube electrode is further confirmed by its changes in the electrochemical redox responses upon hybridization, as shown in figure 18. The strong reductive current peaks seen at 0.29 V in figure 18, attributable to ferrocene [165–167], suggest that the FCA-labelled cDNA chains have been selectively bound onto the ssDNA-grafted aligned carbon nanotube electrode through the hybridization to form a dsDNA structure. The increase in the current peak intensity with the plasma treatment time from 1 min (curve (a) of figure 18) to 5 min (curve (b) of figure 18) indicates the presence of an increased amount of the plasma-induced surface carboxyl groups, and hence the surface-bound DNA chains, in the latter case. The formation of the surface-bound dsDNA chains on the plasma-treated aligned carbon nanotube electrode was also evidenced by a control experiment, carried out with noncomplementary ssDNA chains pre-labelled with FCA (e.g. [FCA-C6]GGTGGCGACTCCTGGAG) under the same conditions, in which only the capacitive current was observed with no apparent peak attributable to the presence of any redox active species. Therefore, the aligned carbon nanotube electrochemical DNA sensors thus demonstrated possess a high sensitivity with capabilities of selectively recognizing DNA sequences.

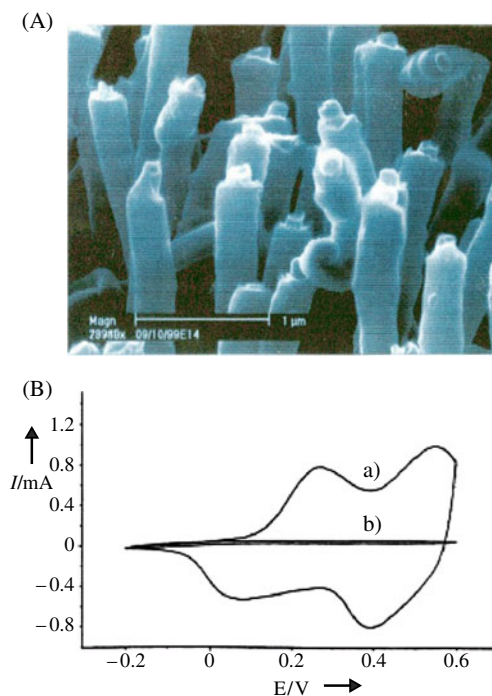


Figure 19. (A) Typical SEM images of the CP-NT coaxial nanowires produced by cyclic voltammetry on the aligned carbon nanotube electrode, showing a thin layer of conducting polymer (polypyrrole) coating surrounding each of the constituent aligned carbon nanotubes. (B) Cyclic voltammograms of (a) the polyaniline-coated CP-NT coaxial nanowires and (b) the bare aligned carbon nanotubes. Measured in an aqueous solution of 1M H₂SO₄ with a scan rate of 50 mV s⁻¹ [54].

3.3.4. Functionalized surfaces with aligned carbon nanotube and conducting polymer coaxial nanowires. In addition to the chemical grafting of polymer chains onto the carbon nanotube surface, we have recently used the aligned carbon nanotubes as nanoelectrodes for making novel conducting coaxial nanowires by electrochemically depositing a concentric layer of an appropriate conducting polymer uniformly onto each of the constituent aligned nanotubes to form the aligned conducting polymer coated carbon nanotube coaxial nanowires (CP-NT) [54] (figure 19 (A)).

The electrochemical performance of the aligned CP-NT coaxial nanowires was evaluated by carrying out cyclic voltammetry measurements. As for polyaniline films electrochemically deposited on conventional electrodes, the cyclic voltammetric response of the polyaniline-coated nanotube array in an aqueous solution of 1 M H₂SO₄ (figure 19 B(a)) shows oxidation peaks at 0.33 and 0.52 V (but with much higher current densities) [168]. This indicates that polyaniline films thus prepared are highly electroactive. As a control, the cyclic voltammetry measurement was also carried out on the bare aligned nanotubes under the same conditions (figure 19 B(b)). In the control experiment, only capacitive current was observed with no peak attributable to the presence of any redoxactive species.

To demonstrate the potential sensing applications for the CP-CNT coaxial nanowires, we have also immobilized glucose oxidase onto the aligned carbon nanotube substrate by electropolymerization of pyrrole in the presence of glucose

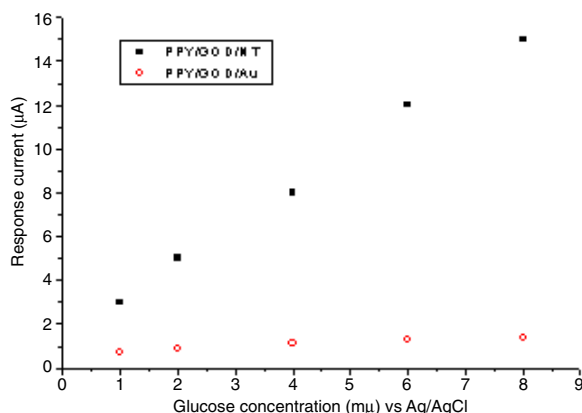


Figure 20. The dependence of electro-oxidation current at the oxidative potential of H_2O_2 on the glucose concentration for the CP-NT coaxial nanowire sensor (solid squares) and the conventional polypyrrole sensor on a flat electrode under the same conditions (open circles) [169].

oxidase [169]. The glucose oxidase-containing polypyrrole-carbon nanotube coaxial nanowires were used to monitor the concentration change of hydrogen peroxide (H_2O_2) generated from the glucose oxidation reaction by measuring the increase in the electro-oxidation current at the oxidative potential of H_2O_2 (i.e. the amperometric method). The amperometric response was found to be much higher than that of more conventional flat electrodes coated with glucose oxidase-containing polypyrrole films under the same conditions.

As shown in figure 20, a linear response of the electro-oxidation current to the glucose concentration was obtained for the CP-NT nanowire sensor. The linear relationship extends to the glucose concentration as high as 20 mM, which is higher than the 15 mM typical for the detection of blood glucose in practice [170]. Furthermore, the amperometric response was found to be about ten orders of magnitude higher than that of more conventional flat electrodes coated with glucose oxidase-containing polypyrrole films under the same conditions [170].

Apart from the large surface/interface area obtained for the nanotube-supported conducting polymer layer, which is attractive for use in sensing applications, the coaxial structure allows the nanotube framework to provide mechanical stability [171, 172] and efficient thermal/electrical conduction [37, 173, 174] to and from the conducting polymer layer. Furthermore, the CP-CNT nanowire sensors were also demonstrated to be highly selective for glucose with their amperometric responses being almost unchanged even in the presence of some interference species including ascorbic acid, urea and D-fructose. Therefore, CP-CNT nanowires could be used for making new glucose sensors with a high sensitivity, selectivity and reliability, which is clearly an area in which future work would be of value.

4. Conclusion

We have demonstrated that surface modification and micro/nano-fabrication play important roles in controlling the properties of a wide range of materials, and in regulating the performance of a large variety of devices. We have focused our attention on the surface functionalization of/by polymers and carbon nanotubes and their use for

modifying various other substrate surfaces for optoelectronic and sensing applications. Even this short paper has revealed the versatility of surface modification and fabrication for making sophisticated materials with good bulk and surface properties and devices with desirable features for specific applications. With so many advanced surface functionalization and device fabrication methods already reported and more to be developed, the examples discussed in this paper will surely be only the first few of many functionalized systems based on polymers and carbon nanotubes attractive for nanotechnological applications.

References

- [1] Ottenbrite R M and Chiellini E (ed) 1992 *Polymers in Medicine: Biomedical and Pharmaceutical Applications* (Lancaster, PA: Technomic Publishing)
- [2] Lovinger A J and Rothberg L J 1996 *J. Mater. Res.* **11** 1581
- [3] Katz H E 1997 *J. Mater. Chem.* **7** 369
- [4] Horowitz G 1998 *Adv. Mater.* **10** 365
- [5] Sariciftci S and Heeger A J 1994 *Int. J. Mod. Phys. B* **8** 237
- [6] Dai L, Dong L, Tong L and Mau A W H 2001 *Adv. Mater.* **13** 915–25 and references cited therein
- [7] Antón P S, Silbergliitt R and Schneider J 2001 *The Global Technology Revolution* (California, USA: Rand)
- [8] Moreau W M 1988 *Semiconductor Lithography: Principle and Materials* (New York: Plenum)
- [9] Jackman R J and Whitesides G M 1999 *CHEMTECH* **18** (May)
- [10] Ulman A 1996 *Chem. Rev.* **96** 1533
- [11] Kim T, Ye Q, Sun L, Chan K C and Crooks R M 1996 *Langmuir* **12** 6065
- [12] Delamarche E, Michel B, Biebuyck H A and Gerber C 1996 *Adv. Mater.* **8** 719
- [13] Hollan J R and Bell A T (ed) 1974 *Techniques and Applications of Plasma Chemistry* (New York: Wiley)
- [14] Yasuda H 1978 *Plasma Polymerization* (Orlando, FL: Academic)
- [15] Agostino R d' 1990 *Plasma Deposition, Treatment, and Etching of Polymers* (San Diego, CA: Academic)
- [16] Martin C R 1995 *Acc. Chem. Res.* **28** 957
- [17] Martin C R 1996 *Chem. Mater.* **8** 1739
- [18] Healey B, Foran S E and Walt D R 1995 *Science* **269** 1078
- [19] Hamers R J 1996 *J. Phys. Chem.* **100** 13103
- [20] Cuberes M T, Schlittler R R and Gimzewski J K 1996 *Appl. Phys. Lett.* **69** 3016
- [21] Wagner C D, Riggs W M, Davis L E, Moulder J F and Muilenberg G E 1979 *Handbook of X-ray Photoelectron Spectroscopy* (Wellesley, MA: Perkin Elmer Corp.)
- [22] Benninghoven A, Rudenauer F G and Werner H W 1987 *Secondary Ion Mass Spectrometry* (New York: Wiley-Interscience)
- [23] Penfold J, Richardson R M, Zarbakhsh A, Webster J R P, Bucknall D G, Rennie A R, Jones R A L, Cosgrove T, Thomas R K, Higgins J S, Fletcher P D I, Dickinson E, Roser S J, McLure I A, Hillman A R, Richards R W, Staples E J, Burgess A N, Simister E A and White J W 1997 *J. Chem. Soc., Faraday Trans.* **93** 3899
- [24] Goldstein A N 1997 *Handbook of Nanophase Materials* (New York: Dekker)
- [25] Iijima S 1991 *Nature* **354** 56
- [26] Tsuruta T, Hayashi T, Kataoka K, Ishihara K and Kimura Y (ed) 1993 *Biomedical Applications of Polymeric Materials* (Boca Raton, FL: Chemical Rubber Company Press)
- [27] Nalwa H S (ed) 1997 *Handbook of Organic Conductive Molecules and Polymers* (New York: Wiley)
- [28] Dai L 1999 *J. Macromol. Sci., Rev. Macromol. Chem. Phys.* **39** 273

- [29] Dresselhaus M S, Deesselhaus G and Eklund P 1996 *Science of Fullerenes and Carbon Nanotubes* (New York: Academic)
- [30] Ebbesen T 1997 *Carbon Nanotubes* (Boca Raton, FL: Chemical Rubber Company Press)
- [31] Saito R, Deesselhaus G and Dresselhaus M S 1998 *Physical Properties of Carbon Nanotubes* (London: Imperial College Press)
- [32] Terrones M, Hsu W K, Hare J P, Kroto H W, Terrones H and Walton D R M 1996 *Phil. Trans. R. Soc. A* **354** 2025
- [33] Yakobson B I and Smalley R E 1997 *Am. Sci.* **85** 325
- [34] Ajayan P M and Ebbesen T W 1997 *Rep. Prog. Phys.* **60** 1026
- [35] Dai L 1999 *Polym. Adv. Technol.* **10** 357
- [36] de Heer W A, Bonard J M, Fauth K, Châtelain A, Forró L and Ugarte D 1997 *Adv. Mater.* **9** 87 and references therein
- [37] Frank S, Poncharal P, Wang Z L and de Heer W A 1998 *Science* **280** 1744
- [38] Dai H, Hafner J H, Rinzler A G, Colbert D T and Smalley R E 1996 *Nature* **384** 147
- [39] Harris J A, Stuart S J, Robertson D H and White C T 1997 *J. Phys. Chem. B* **101** 9682
- [40] Wong S S, Harper J D, Lansbury P T Jr and Lieber C M 1998 *J. Am. Chem. Soc.* **120** 603
- [41] Wong S S, Joselevich E, Woolley A T, Cheung C L and Lieber C M 1998 *Nature* **394** 52
- [42] Che G, Lakshmi B B, Fisher E R and Martin C R 1998 *Nature* **393** 346–9
- [43] Planeix J M, Coustel N, Coq B, Brotons V, Kumbhar P S, Dutartre R, Geneste P, Bernier P and Ajayan P M 1994 *J. Am. Chem. Soc.* **116** 7935
- [44] Guo Z, Sadler P J and Tsang S C 1998 *Adv. Mater.* **10** 701 and references cited therein
- [45] Jirage K B, Hulstee J C and Martin C R 1997 *Science* **278** 655
- [46] Baughman R H, Cui C, Zakhidov A A, Iqbal Z, Barisci J N, Spinks G M, Wallace G G, Mazzoldi A, De Rossi D, Rinzler A G, Jaschinski O, Roth S and Kertesz M 1999 *Science* **284** 1340
- [47] Romero D B, Carrard M, de Heer W and Zuppiroli L 1996 *Adv. Mater.* **8** 899
- [48] Curran S A, Ajayan P M, Blau W J, Carroll D L, Coleman J N, Dalton A B, Davey A P, Drury A, McCarthy B, Maier S and Strevens A 1998 *Adv. Mater.* **10** 1091
- [49] Huang S, Dai L and Mau A W H 1999 *J. Phys. Chem. B* **103** 4223
- [50] Yang Y, Huang S, He H, Mau A W H and Dai L 1999 *J. Am. Chem. Soc.* **121** 10832
- [51] Huang S, Mau A W H, Turney T W, White P A and Dai L 2000 *J. Phys. Chem. B* **104** 2193
- [52] Chen Q and Dai L 2000 *Appl. Phys. Lett.* **76** 2719
- [53] Chen Q and Dai L 2001 *J. Nanosci. Nanotechnol.* **1** 43
- [54] Gao M, Huang S, Dai L, Wallace G, Gao R and Wang Z 2000 *Angew. Chem. Int. Edn Engl.* **39** 3664
- [55] Chen Q, Dai L, Gao M, Huang S and Mau A W H 2001 *J. Phys. Chem. B* **105** 618
- [56] Dai L and Mau A W H 2001 *Adv. Mater.* **13** 899
- [57] Mittal K L and Lee K W (ed) 1997 *Polymer Surfaces and Interfaces: Characterization, Modification and Application* (Utrecht: VSP)
- [58] Fuhrhop J H and Köning J 1994 *Membranes and Molecular Assemblies: the Synkinetic Approach* (London: The Royal Society of Chemistry)
- [59] Galaev I and Mattiasson B 2002 *Smart Polymers for Bioreparation and Bioprocessing* (London: Taylor and Francis)
- [60] Yasuda H 1985 *Plasma Polymerization* (New York: Academic)
- [61] d'Agostino R (ed) 1990 *Plasma Deposition, Treatment, and Etching of Polymers* (New York: Academic)
- [62] Dai L, Griesser H J and Mau A 1997 *J. Phys. Chem. B* **101** 9548 and references cited therein
- [63] Chatelier R, Dai L, Griesser H J, Sheng L, Zientek P, Lohmann D and Chabreck P 1994 *PCT Int. Appl. WO* **94 06 485**
- [64] Singh J and Agrawal K K 1992 *J. Macromol. Sci., Rev. Macromol. Chem. Phys.* **32** 521
- [65] Dai L, Zientek P, St John H, Pasic P, Chatelier R and Griesser H J 1996 *Surface Modification of Polymeric Biomaterials* (New York: Plenum) p 147
- [66] Beamson G and Briggs D 1992 *High Resolution XPS of Organic Polymers: the Scienta ESCA 300 Database* (New York: Wiley)
- [67] Griesser H J, Youxian D, Hughes A E, Gengenbach T R and Mau A W H 1991 *Langmuir* **7** 2484
- [68] Dai L, St John H, Bi J, Zientek P, Chatelier R and Griesser H J 2000 *Surf. Interface Anal.* **29** 46
- [69] Walls J M (ed) 1990 *Methods of Surface Analysis: Techniques and Applications* (Cambridge: Cambridge University Press)
- [70] Osterberg E, Berstrom K, Holmberg K, Schuman T P, Riggs J A, Burns N L, Van Alstine J M and Harris J M 1995 *J. Biomed. Mater. Res.* **29** 741
- [71] Williams D R M 1993 *Macromolecules* **26** 5806
- [72] Iwao T, Langley K H and Karasz F E 1993 *Mater. Res. Soc. Symp. Proc.* **290** 311
- [73] Brochard-Wyart F and de Gennes P G 1994 *J. Macromol. Sci. Macromol. Symp.* **79** 1
- [74] Zhao W, Krausch G, Rafailovich M H and Sokolov J 1994 *Macromolecules* **27** 2933
- [75] Zhulina E and Balazs A C 1996 *Macromolecules* **29** 2667
- [76] Spatz J P, Möller M, Noeske M, Behm R J and Pietralla M 1997 *Macromolecules* **30** 3874
- [77] Wirth M J, Fairbank R W P and Fatunmbi H O 1997 *Science* **275** 44
- [78] Klein J, Perahia D and Warburg S 1991 *Nature* **352** 143
- [79] Seveck E M and Williams D R M 1994 *Macromolecules* **27** 5285
- [80] Okahata Y, Noguchi H and Seki T 1986 *Macromolecules* **19** 494
- [81] Ito Y, Ochiai Y, Park Y S and Imanishi Y 1997 *J. Am. Chem. Soc.* **119** 1619
- [82] Klein J, Kumacheva E, Mahalu D, Perahia D and Fetters L J 1994 *Nature* **370** 634
- [83] Martin J I, Wang Z-G and Schick M 1996 *Langmuir* **12** 4950
- [84] Patel S and Tirrell M 1989 *Annu. Rev. Phys. Chem.* **40**
- [85] Halperin A, Tirrell M and Lodge T P 1992 *Adv. Polym. Sci.* **100** 31
- [86] Milner S T 1991 *Science* **251** 905
- [87] Luckham P F and Costello B A 1993 *Adv. Colloid Interface Sci.* **44** 183
- [88] Napper D H 1983 *Polymeric Stabilization of Colloidal Dispersions* (London: Academic)
- [89] Cantor C R and Schimmel P R 1980 *Biophysical Chemistry* (New York: Freeman)
- [90] Taunton H J, Toprakcioglu C, Fetters L J and Klein J 1990 *Macromolecules* **23** 571
- [91] Taunton H J, Toprakcioglu C, Fetters L J and Klein J 1988 *Nature* **332** 712
- [92] Dai L and Toprakcioglu C 1991 *Europhys. Lett.* **16** 331
- [93] Toprakcioglu C, Dai L, Ansarif M A, Stamm M and Motschmann H 1993 *Prog. Colloid Polym. Sci.* **91** 83
- [94] Dai L, Toprakcioglu C and Hadziioannou G 1995 *Macromolecules* **28** 5512
- [95] Israelachvili J 1992 *Intermolecular and Surface Forces* (London: Academic)
- [96] Toprakcioglu C, Dai L and Ansarif M A 1992 *Macromol. Rep. A* **29** 139
- [97] Field J B, Toprakcioglu C, Dai L, Hadziioannou G, Smith G and Hamilton W J 1992 *J. Physique* **2** 2221

- [98] Field J B, Toprakcioglu C, Ball R C, Stanley H B, Dai L, Barford W, Penfold J, Smith G and Hamilton W 1992 *Macromolecules* **25** 434
- [99] Higgins J S and Benoît H C 1994 *Polymers and Neutron Scattering* (Oxford: Clarendon)
- [100] Auroy P and Auvray L 1992 *Macromolecules* **25** 4134
- [101] Lai P-Y and Halperin A 1992 *Macromolecules* **25** 6693
- [102] Dai L and Toprakcioglu C 1992 *Macromolecules* **25** 6000
- [103] Milner S T and Witten T A 1992 *Macromolecules* **25** 5495
- [104] Tang W H and Witten T A 1996 *Macromolecules* **29** 4412
- [105] Misra S and Mattice W L 1994 *Macromolecules* **27** 2058
- [106] Misra S, Nguyen-Misra M and Mattice W L 1994 *Macromolecules* **27** 5037
- [107] Nguyen-Misra M and Mattice W L 1995 *Macromolecules* **28** 6976
- [108] Nguyen-Misra M, Misra S and Mattice W L 1996 *Macromolecules* **29** 1407
- [109] Björling M and Stilbs P 1998 *Macromolecules* **31** 9033
- [110] Haliloglu T and Mattice W L 1997 *Macromol. Theory Simul.* **6** 667
- [111] Anastassopoulos D L, Vradis A A, Toprakcioglu C, Smith G S and Dai L 1998 *Macromolecules* **31** 9369
- [112] Voivodov K, Chan W-H and Scouten W 1993 *Macromol. Chem., Macromol. Symp.* **70/71** 275
- [113] Ranieri J P, Bellamkonda R, Jacob J, Vargo T G, Gardella J A and Aebischer P 1993 *J. Biomed. Mater. Res.* **27** 917
- [114] Pritchard D J, Morgan H and Cooper J M 1995 *Angew. Chem. Int. Edn Engl.* **34** 91
- [115] Matsuda T and Sugawara T 1995 *Langmuir* **11** 2267
- [116] Matsuda T and Sugawara T 1995 *Langmuir* **11** 2272
- [117] Sugawara T and Matsuda T 1994 *Macromolecules* **27** 7809
- [118] Dai L 2001 *Radiat. Phys. Chem.* **62** 55
- [119] Winkler B, Dai L and Mau A W H 1999 *Chem. Mater.* **11** 704
- [120] Nguyen T P, Le Rendu P, Amgaard K, Cailler M and Tran V H 1995 *Synth. Met.* **72** 35
- [121] Furukawa K, Terasaka Y, Ueda H and Matsumura M 1997 *Synth. Met.* **91** 99
- [122] Wu C C, Sturm J C and Kahn A 1997 *Appl. Phys. Lett.* **70** 1348
- [123] Hu B and Karasz F E 1998 *Chem. Phys.* **227** 263
- [124] Salaneck W R, Stafström S and Brédas J L 1996 *Conjugated Polymer Surfaces and Interfaces* (Cambridge: Cambridge University Press)
- [125] Xu X, Luo X, Xie Y and Zhou H (ed) 1995 *Proc. Int. Workshop Electroluminescence (EL'94)* (Beijing: Science)
- [126] Benson S W and Bose A N 1963 *J. Am. Chem. Soc.* **85** 1385
- [127] Bowden M J and Turner S R 1988 *Electronic and Photonic Applications of Polymers* (*Adv. Chem. Ser.* 218) (Washington, DC: American Chemical Society)
- [128] Dai L and Mau A W H 2000 *J. Phys. Chem. B* **104** 1891–915
- [129] Dai L, Griesser H J, Hong X, Mau A W H, Spurling T H, Yang Y and White J W 1996 *Macromolecules* **29** 282
- [130] Dai L and White J W 1991 *Polymer* **32** 2120
- [131] Dai L 1992 *J. Phys. Chem.* **96** 6469
- [132] Dai L, Mau A W H, Griesser H J and Winkler D A 1994 *Macromolecules* **27** 6728
- [133] Golub M A and Parkinson D B 1968 *Makromol. Synth.* **3** 32
- [134] Colaneri N F, Bradely D D C, Friend R H, Burn P L, Holmes A B and Spangler C W 1990 *Phys. Rev. B* **42** 11670
- [135] Xu B and Holdcroft S 1993 *Macromolecules* **26** 4457
- [136] Bethune D S, Kiang C H, de Vries M S, Gorman G, Savoy R, Vazquez J and Beyers R 1993 *Nature* **363** 605
- [137] Iijima S and Ichihashi T 1993 *Nature* **363** 603
- [138] Ebbesen T W and Ajayan P M 1992 *Nature* **358** 220
- [139] Dai H, Wong E W and Lieber C M 1996 *Science* **272** 523
- [140] Ebbesen T W 1994 *Annu. Rev. Mater. Sci.* **24** 235
- [141] Ebbesen T W, Lezec H J, Hiura H, Bennett J W, Ghaemi H F and Thio T 1996 *Nature* **382** 54
- [142] Thess A *et al* 1996 *Science* **273** 483
- [143] Harris P J F 1999 *Carbon Nanotubes and Related Structures: New Materials for Twenty-first Century* (Cambridge: Cambridge University Press)
- [144] Ajayan P M 1995 *Adv. Mater.* **7** 489
- [145] Ajayan P M, Stephan O, Collix C and Trauth D 1994 *Science* **265** 1212
- [146] de Heer W A, Bacsu W S, Châtelain A, Gerfin T, Humphreybaker R, Forró L and Ugarte D 1995 *Science* **268** 845
- [147] Huang S and Dai L 2002 *J. Nanoparticles Res.* **4** 145–55
- [148] Li D-C, Dai L, Huang S, Mau A W H and Wang Z L 2000 *Chem. Phys. Lett.* **316** 349
- [149] Tsang S C, Chen Y K, Harris P J F and Green M L H 1994 *Nature* **372** 159
- [150] Fan S, Chapline M G, Franklin N R, Tomber T W, Cassell A M and Dai H 1999 *Science* **283** 512
- [151] Li J, Papadopoulos C and Xu J M 1999 *Appl. Phys. Lett.* **75** 367
- [152] Ren Z F, Huang Z P, Wang D Z, Wen J G, Xu J W, Wang J H, Calvet L E, Chen J, Klemic J F and Reed M A 1999 *Appl. Phys. Lett.* **75** 1086
- [153] Suh J S, Lee J S and Jin S 1999 *Appl. Phys. Lett.* **75** 2047
- [154] March J 1992 *Advanced Organic Chemistry* 4th edn (New York: Wiley)
- [155] Wallraff G M and Hinsberg W D 1999 *Chem. Rev.* **99** 1801
- [156] Xia Y and Whiteside G M 1998 *Angew. Chem. Int. Edn Engl.* **37** 550–75
- [157] Bonard J M, Salvétat J P, Stöckli T, de Heer W A, Forró L and Chatelain A 1998 *Appl. Phys. Lett.* **73** 918
- [158] Huang S and Dai L 2002 *J. Phys. Chem. B* **106** 3543
- [159] Dai L, Patil A and Vaia R A 2003 *AIP Conf. Proc.* ed H Kuzmany, J Fink, M Mehring and S Roth (New York: American Institute of Physics)
- [160] Wang J, Cai X, Rivas G, Shiraishi H, Farias P and Dontha N 1996 *Anal. Chem.* **68** 2629
- [161] Kelly S O, Boon E M, Barton J K, Jackson N M and Hill M G 1999 *Nucleic Acids Res.* **27** 4830
- [162] Palecek E and Fojta M 2001 *Anal. Chem.* **73** 74A
- [163] Maruyama K, Mishima Y, Minagawa K and Motonaka J 2002 *Anal. Chem.* **74** 3698
- [164] Cai H, Wang Y, He P and Fang Y 2002 *Anal. Chim. Acta* **469** 165
- [165] Dwyer C, Guthold M, Falvo M, Washburn S, Superfine R and Erie D 2002 *Nanotechnology* **13** 601
- [166] Xu C, He P and Fang Y 2000 *Anal. Chim. Acta* **411** 31
- [167] Nakayama M, Ihara T, Nakano K and Maeda M 2002 *Talanta* **56** 857
- [168] Sazou D and Georgolios C 1997 *J. Electroanal. Chem.* **429** 81
- [169] Gao M, Dai L and Wallace G 2003 *Electroanal. Chem.* **11** 1089
- [170] Yasuzawa M and Kunugi A 1999 *Electrochem. Commun.* **1** 459
- [171] Poncharal P, Wang Z L, Ugarte D and de Heer W A 1999 *Science* **283** 1513 and references cited therein
- [172] Gao R, Wang Z L, Bai Z, de Heer W A, Dai L and Gao M 2000 *Phys. Rev. Lett.* **85** 622
- [173] Odom T W, Huang J-L, Kim P and Lieber C M 2000 *J. Phys. Chem. B* **104** 2794 and references cited therein
- [174] Frank S, Poncharal P, Wang Z L and de Heer W A 1998 *Science* **280** 1744